

ALL OPTICAL CHARACTERIZATION OF A DUAL GRATING ACCELERATOR STRUCTURE

S. Crisp*, A. Ody, P. Musumeci
UCLA, Los Angeles, USA

Abstract

Dielectric laser accelerators have thus far relied on custom nanofabrication of structures. Moving toward MeV scale energy gain requires longer structures which, when made of 2 gratings, are difficult to bond with nm level precision. The efficiency of dual grating structures depends highly on both offset and gap, which has thus far only been measurable by observed transmission and modulation of electrons. We present a structure constructed of commercially available gratings which allow for full flexibility in gap and offset. This structure is then optically characterized, matching diffraction order intensities to simulation results.

INTRODUCTION

The Accelerator on a Chip International Program (ACHIP) seeks to use dielectric laser accelerators (DLAs) to shrink accelerators to the sub-millimeter scale. The nonrelativistic regime has had success in obtaining net acceleration and attosecond bunching using nanofabricated pillar based structures made from B:Si [1, 2]. Fused silica has a high damage threshold for femtosecond-class laser pulses, allowing for GV/m gradients as demonstrated in the relativistic regime [3–5]. These relativistic structures are dual grating structures, meaning they are simple to fabricate in addition to having built-in filtering – electrons that do not get accelerated simply hit the glass, and do not obfuscate a modulation signal.

The ability of the structure to convert input laser intensity into acceleration, known as the structure factor, depends critically on the gap size and relative offset of the gratings. Prior structures have been made by bonding two gratings together[6], which has made characterizing them without the use of an electron beam difficult. Up to now, the only way to probe gap size was to measure transmission with an electron beam and infer offset from structure factor. As the DLA effort drives toward higher interaction lengths and therefore longer structures, characterizing the structures outside of using an electron beam is useful to conserve beam time and compensate for resulting dynamic effects [7, 8].

In this paper, we discuss the optical characterization of a dielectric structure made of 2 independently mounted gratings. Measurements are compared to simulation of the relative weight of the +-1 diffraction lobes off a dual grating structure. The diffraction measurement can be performed in air, with the use of only a small laser diode. In addition, it can also be done in-situ, with the structure installed on the beamline, in order to fine-tune the relative offset of the gratings during a beam-on DLA run.

* sophiecrisp@physics.ucla.edu

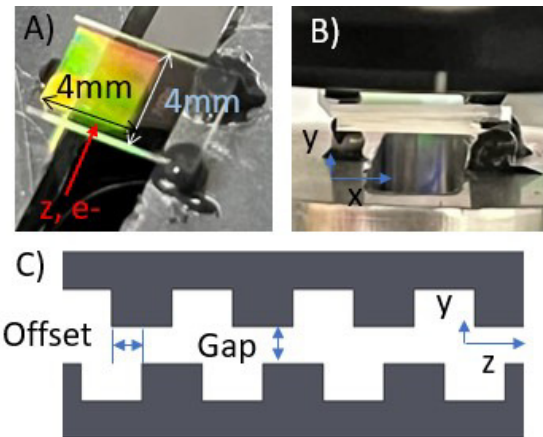


Figure 1: A) The 4 mmx4 mm grating is inset on 5 mmx8 mm x0.625 mm piece of fused silica. The future electron direction is denoted by the z direction, and is perpendicular to the grating direction. This is mounted using an aluminum filled epoxy on three points, one in the center of the grating side, and 2 on the edges away from the grating. This creates a flat plane and minimizes glass warping as the epoxy dries. Holes below and to the sides of the lower grating allow the first diffraction orders to be measured. B) Head on view of the assembled grating structure. C) A schematic defining the relative offset as the distance between opposing grating teeth and gap as the absolute distance between the two gratings.

ASSEMBLY

The DLA structures are constructed using two commercially available gratings, shown in Fig. 1. These gratings have 800 nm periodicity, allowing them to be driven by a 780 nm laser. In order to have full flexibility in grating mounting, a number of motorized and manually controlled degrees of freedom are implemented, as described in Table 1. Simulations indicate that at gaps larger than 800 nm, the structure factor of a DLA is greatly reduced. This scale requires the use of a piezo motor assembly for gap and angle control.

The upper grating sits in a 2-D translation mount, which is itself mounted in a kinematic mount. This allows coarse control of x, x', and z', and fine control of the offset, z. The lower grating sits atop a 3 piezo motor assembly. This is mounted on a vertical translation stage, which is itself attached to a rotation stage. This combination allows fine and coarse control of the gap, y, as well as fine control of every angle, x', y', and z'. The only dimension not finely controlled via motor is x; this is set by a finely threaded

Table 1: List of all the available degrees of freedom in the fully mounted gratings described in order from top to bottom. X, y, and z refer to the relative displacement between the two gratings; z corresponds to offset and is the beam direction and y corresponds to gap.

Component	Dimension	Control	Range	Resolution
a: Kinematic Mount	x', z'	3 100 TPI Screws	x', z': ±50 mrad	
b: 2-D Translation Mount	x, z	x: 100 TPI Screw z: Stepper motor	x: 2 mm z: 2 mm	z: 0.25 μm
c: Piezo Mount	y, x', z'	3 Piezo Motors	y: 12 μm x', z': ±1.2 mrad	y: 0.4 nm x', z': 0.1 μrad
d: Translation Mount	y	Micrometer	2 mm	1 μm
e: Rotation Mount	y'	Micrometer	±120 mrad	1 mrad

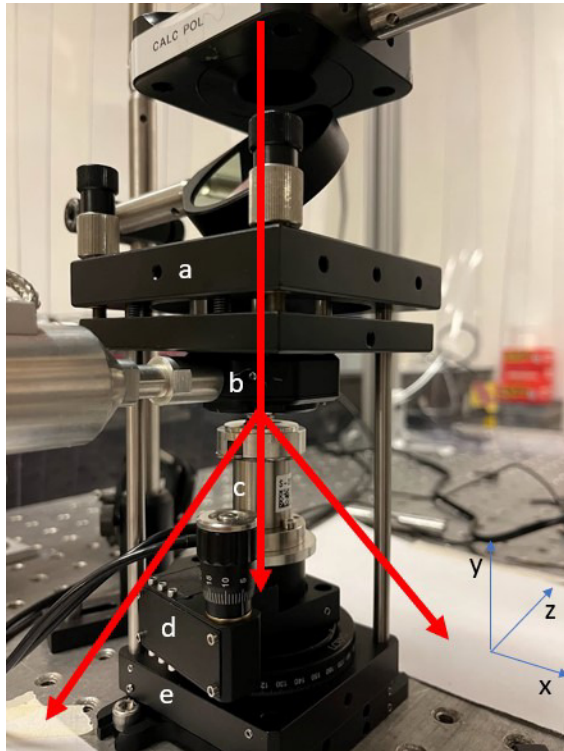


Figure 2: A 635 nm diode laser is incident from above and goes through a polarizer and then beam splitter before hitting the grating assembly. The zeroth order reflected spot can be viewed via the beam splitter reflection. The first order transmitted spots diffract to paper on either side of the grating assembly and are viewed by a camera looking from above. Component labels correspond to Table 1.

screw to maximally overlap the etched section of the silica piece.

To begin assembly, the gratings are attached to their respective mounts at three points with an epoxy, and then put together into a 60 mm cage system with a large gap of 3 mm. Then, a 635 nm laser with 3 mm spot size is input perpendicularly from above, as seen in Fig. 2. The reflected $m=0$ spots are visible, redirected by the beamsplitter. When the gratings are first installed, the reflected spots are clearly visible far from one another; by using the top kinematic mount they can be overlapped. The kinematic mount is used to bring

the gap size to less than 1 mm while retaining the overlap of the reflected spot. As the gratings get closer to one another, thin film interference in the reflected spot starts to become visible.

This interference is in the form of flat, dark fringes in the reflected spot. These represent deviations from flatness by $\lambda/2$; their width is indicative of the slope between glass, and the linearity is representative of the surface flatness. For example, if there are 10 visible fringes across the grating in the reflected interference, this corresponds to a $3.175 \mu\text{m}$ deviation, or $z' = 794 \mu\text{rad}$. Before the piezo motor can be used for final flatness and gap tuning, the kinematic mount must be used to bring the flatness within $0.2 \mu\text{rad}$. Finally, the rotation y' is set by removing interference from the diffracted laser spots.

ABSOLUTE GAP MEASUREMENT

Before moving to diffraction, a reference gap position must be found. The zero gap position where the two gratings are fully in contact with one another is the only intrinsic reference position available. To measure this, the $m=0$ order reflection spot is viewed as gap size is changed by the translation mount. The laser is apertured such that the spot size is $400 \mu\text{m}$ at the structure, and only the flat glass is sampled, not the grating. When the reflected spot no longer changes in tandem with the gap adjustment, the micrometer is backed out about $5 \mu\text{m}$. At this point the piezo motors can be used for fine adjustment.

Using a camera to measure the intensity of the reflected spot, a scan over gap is taken. The angle between gratings is optimized to maximize difference between maximum and minimum intensity. After this optimization, a final scan is performed, as seen in Fig. 3. The behavior here is that of an etalon with low reflectance R ; the transmittance function is given by

$$T = \frac{1}{1 + \frac{4R}{(1-R)^2} \sin^2\left(\frac{\delta}{2}\right)} \quad (1)$$

where the phase shift incurred when the input laser with wavelength λ is perpendicular to the surface is given by

$$\delta = \left(\frac{2\pi}{\lambda}\right) 2nl. \quad (2)$$

Content from this work may be used under the terms of the CC BY 4.0 licence (© 2022). Any distribution of this work must maintain attribution to the author(s), title of the work, publisher, and DOI

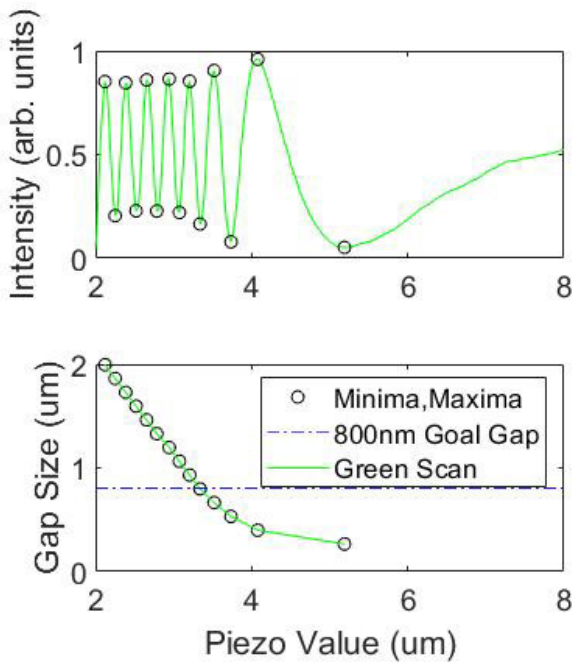


Figure 3: On top, a measurement of the intensity of the $m=0$ order reflected spot of a 532 nm diode as it changes with gap size. Below, piezo value is plotted against inferred actual gap. There is a clear linear regime in which peak to peak distance is the expected 266 nm, after which deformation appears and piezo value no longer correlates directly with gap size. The desired 800 nm gap occurs before this nonlinear regime.

The refractive index n is 1 and l is the gap size. Figure 3 shows the sinusoidal intensity curve over the course of a gap scan. When the piezo motor hits about $3.5 \mu\text{m}$, it appears that deformation begins to occur. Assuming there would be one additional minima, at the actual 0 gap position, one can infer the absolute gap size. It is critical that there is no deformation at the 800 nm to ensure flatness across the structure during acceleration runs.

OFFSET-GAP SCAN

Once the zero gap position is found, the input laser diode is switched to $\lambda = 635 \text{ nm}$ and moved to be incident on the grating. The diffraction spots are viewed on two pieces of paper on either side of the DLA structure. An overhead camera records the intensity of the $m=-1, +1$ order diffraction spots. A scan over gap is performed by moving the piezo motor in small increments, after which the offset stepper motor is moved by at least 100 nm.

Lumerical simulation and diffraction measurement results for a 2-D scan in gap and offset are seen in Fig. 4. Because the diffraction intensities are periodic, this diagnostic can be used only to give relative gap size. However, one can combine this data with a known zero gap position to find the absolute gap. By comparing simulation to data, the offset and therefore the structure factor of the double grating can be extracted. With a gap size of 800 nm and offset of -300 nm

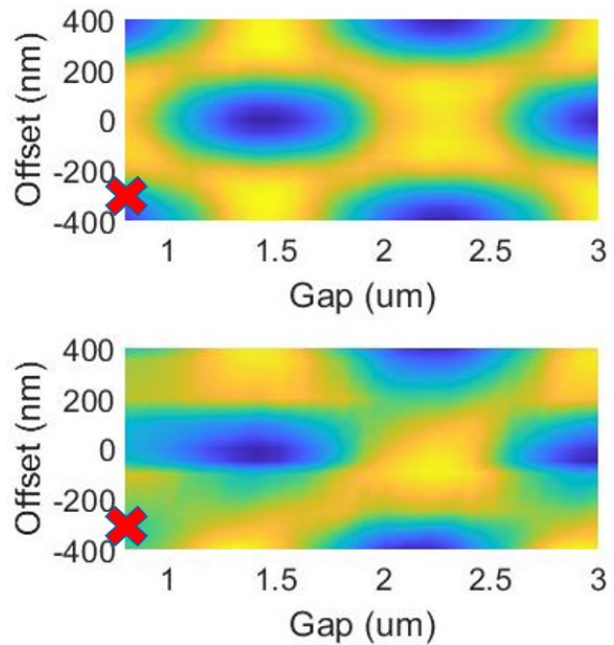


Figure 4: On top, simulation results of a 635 nm linearly polarized beam diffracting through a fused silica double grating structure. Polarization is set perpendicular to the structure. The $m=+1$ and $m=-1$ diffraction intensities are added together to acquire the scans above. Scans over gap and offset on bottom are compared to simulation to fit to offset and relative gap. There is good qualitative agreement between data and simulation. Red x's designate the location of optimal accelerator parameters.

the structure factor, or ratio of peak gradient to incident field, is maximal with a value of 0.16.

CONCLUSION

A fully flexible commercial grating based DLA structure has been assembled and optically characterized. The relative intensity of diffraction spots of a low power laser diode are used to find the offset and gap between two independently mounted gratings. This can be used to assemble DLA structures prior to beamline access or in-situ to tune for optimal offset during runs. This is a key step in developing longer accelerator structures to enable higher interaction lengths, and therefore MeV scale acceleration in DLA structures.

ACKNOWLEDGEMENTS

This work has been supported by the ACHIP grant from the Gordon and Betty Moore Foundation (GBMF4744) and by U.S. Department of Energy grant DE-AC02-76SF00515. This material is based upon work supported by the National Science Foundation Graduate Research Fellowship Program under Grant No. DGE-203483. Any opinions, findings, and conclusions or recommendations expressed in this material are those of the author(s) and do not necessarily reflect the views of the National Science Foundation.

REFERENCES

- [1] D. S. Black *et al.*, “Net acceleration and direct measurement of attosecond electron pulses in a silicon dielectric laser accelerator,” *Phys. Rev. Lett.*, vol. 123, p. 264802, 26 2019, doi:10.1103/PhysRevLett.123.264802
- [2] U. Niedermayer, D. S. Black, K. J. Leedle, Y. Miao, R. L. Byer, and O. Solgaard, “Low-energy-spread attosecond bunching and coherent electron acceleration in dielectric nanostructures,” *Phys. Rev. Applied*, vol. 15, p. L021002, 2 2021, doi:10.1103/PhysRevApplied.15.L021002
- [3] E. A. Peralta *et al.*, “Demonstration of electron acceleration in a laser-driven dielectric microstructure,” *Nature 2013 503:7474*, vol. 503, no. 7474, pp. 91–94, 2013, doi:10.1038/nature12664
- [4] D. Cesar *et al.*, “High-field nonlinear optical response and phase control in a dielectric laser accelerator,” *Communications Physics*, vol. 1, no. 1, p. 46, 2018, doi:10.1038/s42005-018-0047-y
- [5] S. Crisp, A. Ody, P. Musumeci, and R. J. England, “Resonant phase matching by oblique illumination of a dielectric laser accelerator,” *Phys. Rev. Accel. Beams*, vol. 24, p. 121305, 12 2021, doi:10.1103/PhysRevAccelBeams.24.121305
- [6] E. A. Peralta *et al.*, “Design, fabrication, and testing of a fused-silica dual-layer grating structure for direct laser acceleration of electrons,” in *AIP Conference Proceedings*, vol. 1507, 2012, pp. 169–177, doi:10.1063/1.4773690
- [7] U. Niedermayer, T. Egenolf, O. Boine-Frankenheim, and P. Hommelhoff, “Alternating-phase focusing for dielectric-laser acceleration,” *Phys. Rev. Lett.*, vol. 121, p. 214801, 21 2018, doi:10.1103/PhysRevLett.121.214801
- [8] D. Cesar *et al.*, “Enhanced energy gain in a dielectric laser accelerator using a tilted pulse front laser,” *Opt. Express*, vol. 26, no. 22, pp. 29216–29224, 2018, doi:10.1364/OE.26.029216